Core plasma density fluctuations in Wendelstein 7-X ECRH plasmas

J.-P. Bähner[1], J. A. Alcusón[1], S. K. Hansen[2], A. v. Stechow[1], O. Grulke[1,3], T. Windisch[1], H. M. Smith[1], Z. Huang[2], E. M. Edlund[4], M. Porkolab[2], M. N. A. Beurskens[1], S. A. Bozhenkov[1], O. P. Ford[1], L. Vanó[1], A. Langenberg[1], N. Pablant[5], and The W7-X Team[1]

[1]*Max Planck Institute for Plasma Physics, Greifswald, Germany*

[2]*MIT Plasma Science and Fusion Center, Cambridge, MA, USA*

[3]*Technical University of Denmark, Kongens Lyngby, Denmark*

[4]*SUNY Cortland, Cortland, NY, USA*

[5]*Princeton Plasma Physics Laboratory, Princeton, NJ, USA*

Introduction

The Wendelstein 7-X (W7-X) stellarator was optimised for reduced neoclassical transport, which was proven to be successful in the first experiment campaigns [1, 2]. Accordingly, anomalous transport becomes more important for the global confinement and the focus of interest shifts towards turbulence. As part of the efforts to understand the nature of turbulence in W7-X and eventually its role for transport, this work investigates turbulent core density fluctuations in regular discharges of W7-X experimentally via phase contrast imaging (PCI) [3, 4] in combination with gyrokinetic simulations with the code GENE [5].

Radial localisation of density fluctuations

A gas-fuelled hydrogen discharge with 3.2 MW of electron cyclotron heating in the standard magnetic configuration is investigated as a representative reference case for the majority of experiments in the last operation phase. There is no direct ion heating in this type of discharge and the ion temperature remains low and relatively flat throughout the plasma core, while the electron temperature is centrally peaked. The plasma density profile is flat over most of the plasma radius. Fig. 1 shows the experimental time averaged profiles and corresponding normalised gradient length scales.

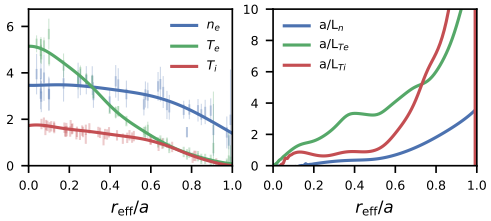

Figure 1: Experimental plasma density and temperature profiles and corresponding normalised gradient length scales of W7-X XP:20180906.38, 4.5s-6.5s

The PCI diagnostic measures line integrated electron density fluctuations through the whole plasma with a temporal and spatial resolution that allows for the measurement of low frequency

ion scale turbulence and a simultaneous wavenumber and frequency (kf) analysis. The measurement direction of the spatial resolution is perpendicular to the line of sight and roughly poloidal. Fig. 2 shows a wavenumber-frequency spectrum of the reference discharge. Opposing propagation directions with respect to the measurement direction are reflected by positive and negative wavenumbers. In both wavenumber branches, it is observed that a large fraction of the spectral power is carried by fluctuations with the same phase velocity in the measurement direction, $v_{\mathrm{ph}}^{\mathrm{PCI}}$. It reflects a projection of the fluctuations propagation velocity in the binormal direction onto the measurement direction,

$$v_{\mathrm{ph}}^{\mathrm{PCI}} = \mathbf{u}_y \cdot \hat{\mathbf{e}}_{\mathrm{m}}, \tag{1}$$

where the former, u_y, is a combination of the mode's phase velocity in the plasma frame, $v_{\mathrm{ph}}^{\mathrm{ITG}}$, and a Doppler-shift by the $E \times B$ rotation of the plasma,

$$u_y = v_{\mathrm{ph}}^{\mathrm{ITG}} + v_{E\times B} \approx v_{E\times B}. \tag{2}$$

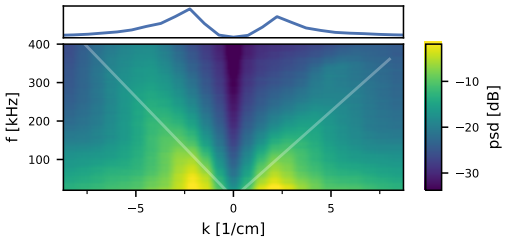

Figure 2: Experimental kf-spectrum by PCI with dominant phase velocities and wavenumber spectrum (top panel).

The $E \times B$ velocity is generally much larger that the phase velocity of the turbulent modes [6, 7, 8]. A single dominant phase velocity in the wavenumber-frequency spectrum therefore implies, that most of the fluctuations are localised at a certain radius such that the $E \times B$ velocity at that radius determines the observed $v_{\mathrm{ph}}^{\mathrm{PCI}}$.

For a direct comparison to the $E \times B$ velocity at the position of the PCI measurement, neoclassical simulations with the code DKES [9] are used to obtain the ambipolar radial electric field, which generally agrees well with measurements by Doppler-reflectometry (DR) and other diagnostics [8, 10, 11] (see fig. 3). The local $E \times B$ velocity is then obtained by

$$v_{E\times B} = \langle E_r \rangle^{\mathrm{NC}} |\nabla r_{\mathrm{eff}}| / B, \tag{3}$$

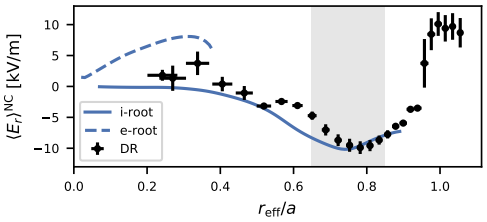

Figure 3: Radial electric field measurements by Doppler-reflectometry (DR) and a DKES simulation.

where $\langle E_r \rangle^{\mathrm{NC}}$ is the flux-surface averaged value simulation output, B is the magnetic field strength and $|\nabla r_{\mathrm{eff}}|$ accounts for the flux compression.

A direct comparison is only valid between $v_{E\times B}$ and u_y. Therefore the projection described in eq. (1) has to be inverted, which depends on the position along the PCI line of sight and even slightly varies across it. Fig. 4 shows the comparison of the inferred u_y (black) and $v_{E\times B}$ (blue).

The faded blue and black lines represent the variation across the PCI laser beam, colour weighted by the respective laser amplitude. The red mark is the phase velocity of the most dominant mode obtained from linear gyrokinetic simulations added to the $E \times B$ velocity in order to illustrate the approximation in Eq. 2. The quantities match best at a radial position of $r_{\text{eff}}/a \approx 0.75$, at the well of the ion root solution. The match implies that this is the radial location where the strongest fluctuations arise.

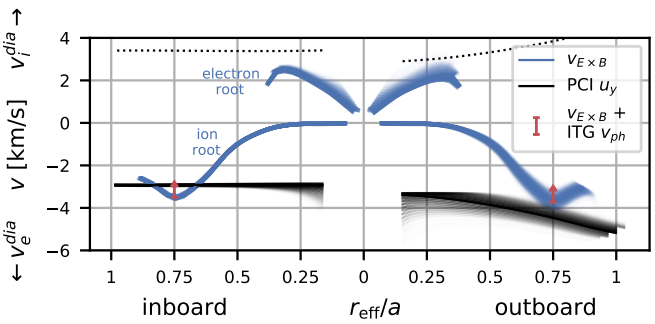

Figure 4: Comparison of binormal velocity corresponding to dominant phase velocity in the PCI spectrum and local $E \times B$ velocity along the PCI line of sight.

Gyrokinetic simulations with GENE

Linear simulations for several positions along the plasma radius were performed for a detailed analysis of the radial evolution of microinstabilities. Idealised profiles based on the experimental reference case were used as input to the simulations. It is found that the electron temperature gradient contribution is dominant for most of the plasma and even for intermediate scales. However, it is worthwhile running simulations without an electron temperature gradient ($a/L_{Te} = 0$) in order to investigate ITG and TEM only, which generally determine the ion scale fluctuations non-linearly. A clear picture arises in these simulations in normalised units: The ITG mode is dominant (over TEM) at all radii and the growth rate increases with increasing effective radius, which strictly follows the evolution of a/L_{Ti}, the driving term for ITG modes. The normalisation strongly depends on the ion temperature, which is why the picture changes in real units. At the very edge, the growth rate is reduced and the dominant mode moves to higher wavenumbers. Ultimately, the ion-scale growth rate peaks at $r_{\text{eff}}/a \approx 0.7$, which supports the experimentally observed localisation from the perspective of linear microinstabilities. In order to simulate density fluctuations, non-linear simulations are needed. Flux-tubes that intersect the PCI line of sight at three different radial locations were chosen and the corresponding gradients of the experimental profiles (fig. 1) used

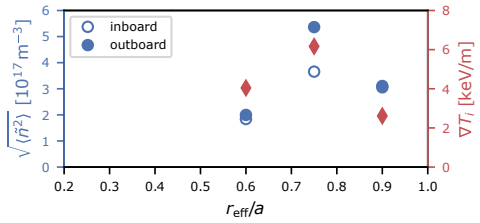

Figure 5: Local density fluctuations from non-linear GENE flux-tube simulations and ion temperature gradient.

as input. Furthermore, the simulations were electrostatic, collisionless and both ions and electrons were treated kinetically. Fig. 5 shows the density fluctuations at the location of the PCI line of sight on the inboard and outboard side. We find additional support for the radial localisation, because in the flux-tube at $r_{\text{eff}}/a = 0.75$ the density fluctuations are the strongest. Additionally, there is a difference between the inboard and outboard side at this radial location, which is observed in the experimental kf-spectrum of PCI (fig. 2). The ion temperature gradient is shown alongside the density fluctuations in order to illustrate the close connection to the dominant drive of turbulence in this radial region.

Conclusion

Density fluctuations in regular W7-X discharges are characterised by a dominant ITG-drive and a radial localisation at $r_{\text{eff}}/a \approx 0.75$, which generally is the same radial region as the E_r-well. This can be shown experimentally and in gyrokinetic simulations (for more details, see [12]). TEMs play a minor role at all radii and scales. ETG is linearly strong but not observed in the outer half of the plasma experimentally or in non-linear simulations.

Acknowledgements

This work is partly sponsored by the US Department of Energy, Office of Fusion Energy Sciences under grant number DE-SC0014229. This work has been carried out within the framework of the EUROfusion Consortium and has received funding from the Euratom research and training programme 2014–2018 and 2019–2020 under grant agreement No 633053. The views and opinions expressed herein do not necessarily reflect those of the European Commission. S. K. Hansen acknowledges support by an Internationalisation Fellowship (CF19-0738) from the Carlsberg Foundation.

References

[1] T. Klinger *et al.*, Nucl. Fusion **59** (11), 112004 (2019)
[2] R. C. Wolf *et al.*, Phys. Plasmas **26** (8), 082504 (2019)
[3] E. Edlund *et al.*, Rev. Sci. Instrum. **89** (10), 10E105 (2018)
[4] Z. Huang *et al.*, J. Instrum. **16** (01), P01014 (2021)
[5] F. Jenko *et al.* Phys. Plasmas **7** (5), 1904–1910 (2000)
[6] G. D. Conway *et al.*, Phys. Rev. Lett. **106**, 065001 (2011)
[7] T. Windisch *et al.*, Rev. Sci. Instrum. **89** (10), 10H115 (2018)
[8] D. Carralero *et al.*, Nucl. Fusion **60** (10), 106019 (2020)
[9] S. P. Hirshman *et al.*, Phys. Fluids **29** (9), 2951–2959 (1986)
[10] N. Pablant *et al.*, Phys. Plasmas **25** (2), 022508 (2018)
[11] O. Ford *et al.*, Rev. Sci. Instrum. **91** (2), 023507 (2020)
[12] J.-P. Bähner *et al.*, J Plasma Phys. (2021) *accepted*